Enhanced superconductivity in the Se-substituted 1T-PdTe₂

Wenhao Liu [1], Sheng Li,[1] Hanlin Wu [1], Nikhil Dhale,[1] Pawan Koirala,[1] and Bing Lv [1,2,*]

¹Department of Physics, University of Texas at Dallas, Richardson, Texas 75080, USA

²Department of Materials Science and Engineering, University of Texas at Dallas, Richardson, Texas 75080, USA

The two-dimensional transition metal dichalcogenide PdTe₂ has recently attracted much attention due to its phase coexistence of a type-II Dirac semimetal and type-I superconductivity. Here we report a 67% enhancement of the superconducting transition temperature in 1T-PdSeTe in comparison to that of PdTe₂ through partial substitution of Te atoms by Se. The superconductivity has been unambiguously confirmed by the magnetization, resistivity, and specific heat measurements. 1T-PdSeTe shows type-II superconductivity with large anisotropy and a nonbulk superconductivity nature with a volume fraction of $\approx 20\%$ estimated from magnetic and heat capacity measurements. 1T-PdSeTe expands the family of superconducting transition metal dichalcogenides and thus provides additional insights for understanding superconductivity and topological physics in the 1T-PdTe₂ system

I. INTRODUCTION

Recently, two-dimensional (2D) materials, including transition metal dichalcogenides (TMDs), have received considerable attention due to their emergent physical properties, which in turn have the potential to revolutionize many fields in both fundamental science and technological applications [1–4]. For example, a large current on-off ratio exceeding an order of 10^8 and ultrahigh mobility are found in MoS₂ [5]. Large transverse magnetoresistance induced by chiral anomaly was observed in MoTe₂ and WTe₂ [6,7], and 2D magnetism down to atomic layers, such as VSe₂, exists [8,9]. The studies of superconductivity through chemical intercalation/doping and the interplay with different sets of charge density wave (CDW) orders have stimulated many research interests since the 1970s [10–15]. Recently, such studies have been extended to electrostatic gating where both T_c and the CDW transition could be significantly tuned through the gating voltage [16–19]. Further studies on the TMDs at the atomically thin layer limit resulted in the Ising pairing in NbSe₂ and Wigner crystal and minibands or other exotic states in twisted-angle TMD heterostructures [20–23].

Structurally, TMDs are constructed by either octahedral or trigonal prismatic MX_2 layers, where M is a transition metal from elements in groups 4 to 10 and X is a chalcogen. There is strong X-M-X bonding within each layer but a rather weak van der Waals interaction between different layers, which result in the easily exfoliable nature for most TMD materials. The variations of stacking sequences of MX_2 layers as well as the atomic coordination often lead to different polytype and polymorphic structures. Based on the numbers of layers in the unit cell and their symmetry, the most common polytypes are 1T (T indicates trigonal), 1T' (distorted 1T), 2H (H indicates

hexagonal), and 3R (R indicates rhombohedral). Among these different TMDs, PdTe₂ has attracted much attention lately as it has been experimentally verified as a type-II Dirac semimetal [24,25].

Dirac semimetals show a Dirac cone where a valence band and a conducting band touch each other at one point (Dirac point) in the energy-momentum space. The low-energy quasiparticle excitation near the Dirac point is called a Dirac fermion, which can be well described by a relativistic Dirac equation. Remarkably, superconductivity was also discovered in the PdTe₂ system [26]. Specific heat and dc magnetization measurements reveal that PdTe₂ is a conventional type-I superconductor with a transition temperature of ~ 1.64 K [27,28]. In addition, a new type of Ising superconductivity was found in an ambient-stable PdTe₂ film with in-plane centrosymmetry, showing a large in-plane critical field more than 7 times the Pauli limit [29]. The simultaneously robust superconductivity and the nontrivial topological states make PdTe₂ a great potential candidate in electronic applications, such as the realization of topological superconductors, which can be used in fault-tolerant quantum computing and could potentially lead to important technological applications. In this paper, we report our research effort to further enhance the superconductivity in the topological PdTe₂ system through chemical doping, and we find significantly enhanced superconductivity in Se-doped 1T-PdSeTe. The structure was confirmed by powder x-ray diffraction, which suggests 1T-PdSeTe is crystallized in the same CdI_2-type structure with space group $P\bar{3}m1$ (164) as its PdTe₂ counterpart. Magnetization revealed large anisotropic superconducting shielding fractions along different magnetic orientations. Specific heat measurements along with magnetization further demonstrate nonbulk feathers of the superconductivity in 1T-PdSeTe. The superconducting phase transition temperature T_c, determined from the resistivity results, is 2.74 K, which is about 67% enhanced compared to that of PdTe₂. The discovery of

*blv@utdallas.edu

superconducting 1T-PdSeTe expands the superconducting TMD family and could provide another planform to study nontrivial topological superconductivity in the TMDs.

II. EXPERIMENT DETAILS

1T-PdSeTe was first reported in 1965 [30]. Our 1T-PdSeTe specimens were synthesized by a self-flux method through melting a stoichiometric amount of Pd (99.95%, Alfa Aesar), Se (99.999%, Alfa Aesar), and Te (99.999%, Alfa Aesar). Small Pd ingots, Se shots, and Te pieces in stoichiometric ratio were weighed inside an Ar glove box with a total moisture and oxygen level less than 0.1 ppm. Se shots and Te pieces were ground into fine powders and loaded inside the silica tube together with Pd ingots. The silica tube was flame sealed under vacuum and placed in a single-zone furnace. The assembly was slowly heated up to $800\,^\circ$C, held for 3 days, then followed by furnace cooling to room temperature. Sizeable shiny and plateletlike crystals (up to 3 mm in size) with preferred crystallographic c axis orientation were obtained by cleaving the ingot product.

Powder x-ray diffraction (XRD) measurements were performed on crushed crystals using a Rigaku SmartLab x-ray diffractometer equipped with Cu $K\alpha$ radiation at room temperature, and Rietveld refinement was carried out using GSAS-II [31]. Scanning electron microscopy (SEM) with energy dispersive x-ray analysis was performed using a Zeiss-LEO 1530. Measurement of dc magnetization was conducted with a Quantum Design magnetic property measurement system down to 1.8 K. Four gold wires (50 μm in diameter) were pasted on the freshly cleaved sample surface by silver epoxy as four probes. Resistivity was measured with a four-probe method using a Quantum Design physical property measurement system (PPMS) down to 1.8 K. Specific heat measurement was done in the PPMS by a time-relaxation method with magnetic field parallel to the crystallographic c axis.

III. RESULTS

The x-ray diffraction patterns for different crystals from the same batch are nearly identical and show only (00l) peaks; that is, the crystallographic c axis is the preferred orientation, as shown in the inset of Fig. 1. This indicates that the c direction is perpendicular to the flat surface of platelet-shaped crystals. The full Rietveld refinement of powder x-ray diffraction on crushed powders from the single crystals is shown in Fig. 1, which establishes that PdSeTe indeed adopts the same crystal structure as 1T-PdTe$_2$ in the trigonal space group $P\bar{3}m1$ (164). Good refinement values of $R_p = 1.91\%$ and $R_{wp} = 3.72\%$ indicate good agreement of experimental data with the refined structural model and the high quality of our samples. Detailed refinement results with the associated Wyckoff position of each atom are shown in Table I. The refined lattice parameters are $a = b = 3.9029(8)$ Å, $c = 4.980(1)$ Å, $\alpha = \beta = 90^\circ$, and $\gamma = 120^\circ$ for 1T-PdSeTe. These values are a bit lower than those of isostructural PdTe$_2$ ($a = b = 4.03$ Å, $c = 5.12$ Å) as expected since Te atoms are replaced by smaller Se atoms in the unit cell. Refined occupancies of Se and Te are 0.47(2) and 0.53(2), respectively, and very close
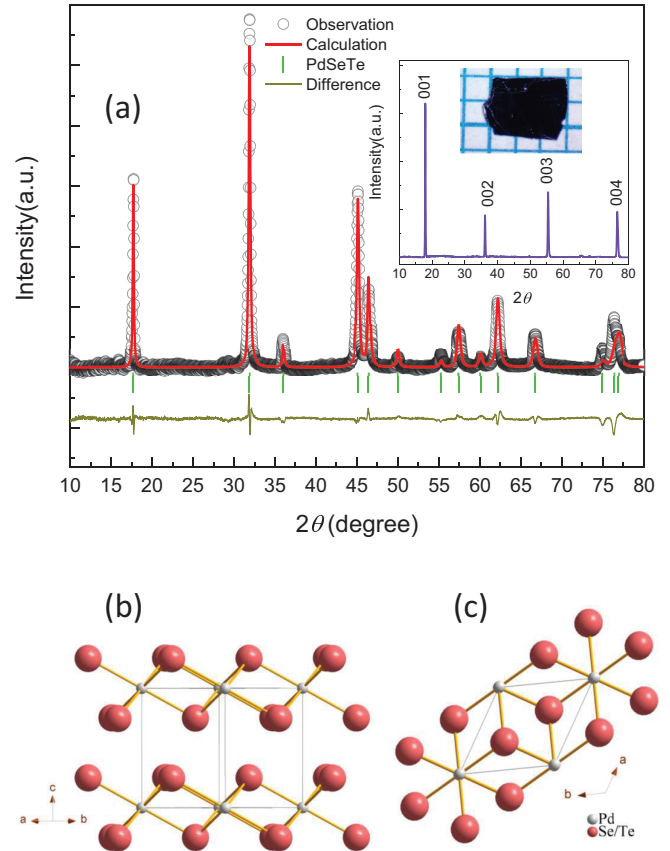

FIG. 1. (a) XRD pattern and Rietveld refinement of 1T-PdSeTe at room temperature. Vertical marks (green bars) stand for positions of Bragg peaks. The inset shows the XRD pattern and optical image on the millimeter-size grid of the easily exfoliated flake. Ball and stick model of the crystal structure of 1T-PdSeTe showing (b) the side view and (c) top view.

to the nominal Se:Te ratio. Figures 1(b) and 1(c) show ball and stick models of the crystal structure of 1T-PdSeTe from the refinement results. The Pd atom is found in octahedral coordination with Se/Te atoms in each layer, and every layer

TABLE I. Summary of crystallographic data and structure refinement parameters for 1T-PdSeTe.

Parameter	Value
Space group	$P\bar{3}m1$
a (Å)	3.9029(8)
b (Å)	3.9029(8)
c (Å)	4.980(1)
V (Å^3)	65.699(4)
D_{cal} (g/cm^3)	7.94
R_p (%)	1.91
R_{wp} (%)	3.72

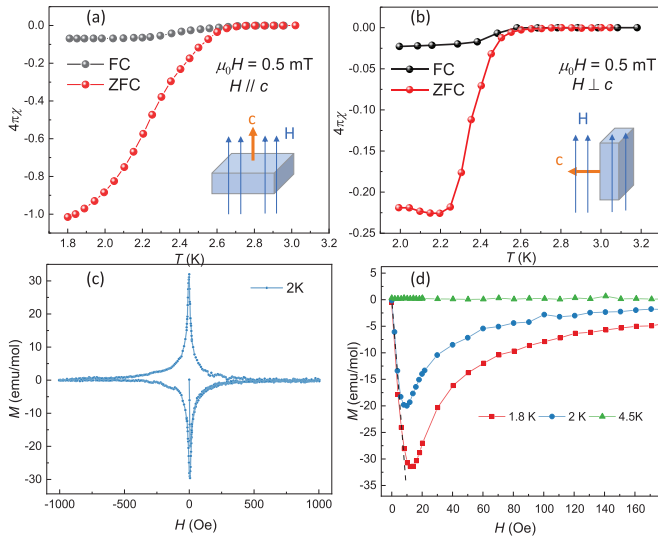| Atom	Site	Symmetry	x/a	y/b	z/c	Occupancy
Pd1	1a	$\bar{3}m$	0	0	0	1
Se1	2d	$3m$	1/3	1/3	0.2537(3)	0.47(2)
Te1	2d	$3m$	1/3	1/3	0.2537(3)	0.53(2)

FIG. 2. Temperature dependence of magnetic susceptibility measured in both the ZFC mode and FC mode with an external field of 5 Oe (a) parallel to the crystallographic c axis and (b) perpendicular to the c axis. (c) Magnetic hysteresis loop of 1T-PdSeTe at 2 K with external field parallel to the c axis. (d) MHLs in the magnetic penetration process at 1.8, 2, and 4.5 K with external field parallel to the c axis. The dashed line represents the slope of the perfect diamagnetism.

stacks repeatedly via van der Waals forces along the c axis of the trigonal unit cell. SEM analysis of crystals on multiple points shows only the existence of Pd, Se, and Te elements in the crystals, and energy-dispersive x-ray spectroscopy shows a ratio of Pd:Se:Te = 1:0.92:1, consistent with Rietveld refinement results, and suggests slight Se vacancies might exist in our samples.

Figures 2(a) and 2(b) illustrate temperature-dependent magnetic susceptibility measured in zero-field-cooled (ZFC) and field-cooled (FC) modes under an external field of 5 Oe parallel to the crystallographic c axis and perpendicular to the c axis, respectively. A clear superconducting transition can be seen in both modes. When magnetic field is parallel to the c axis with the large demagnetization enhancement factor, a large shielding volume fraction of $\sim$102% at 1.8 K is observed using an estimated density of 7.92 g/cm^3. However, when the magnetic field is parallel to the a-b plane where the demagnetization enhancement factor is minimized, the actual shielding fraction we obtained is only about 20% for the same crystal, reflecting the real superconducting volume fraction is less than 100% and a nonbulk superconductivity nature exists in this system. Further annealing the crystals at 500 °C for a few days does not improve the superconducting volume fraction. In Fig. 2(c), we show the magnetization hysteresis loop (MHL) of 1T-PdSeTe at 2 K with a magnetic field applied parallel to the c axis. Figure 2(d) shows MHLs in the magnetic penetration process at 1.8, 2, and 4.5 K with a magnetic field applied parallel to the c axis. The shielding behavior is suppressed with increasing temperature and disappears when the temperature is higher than T_c. Fully penetrating fields corresponding to the maximum value of magnetization are only about 10 Oe at 1.8 K. This suggests
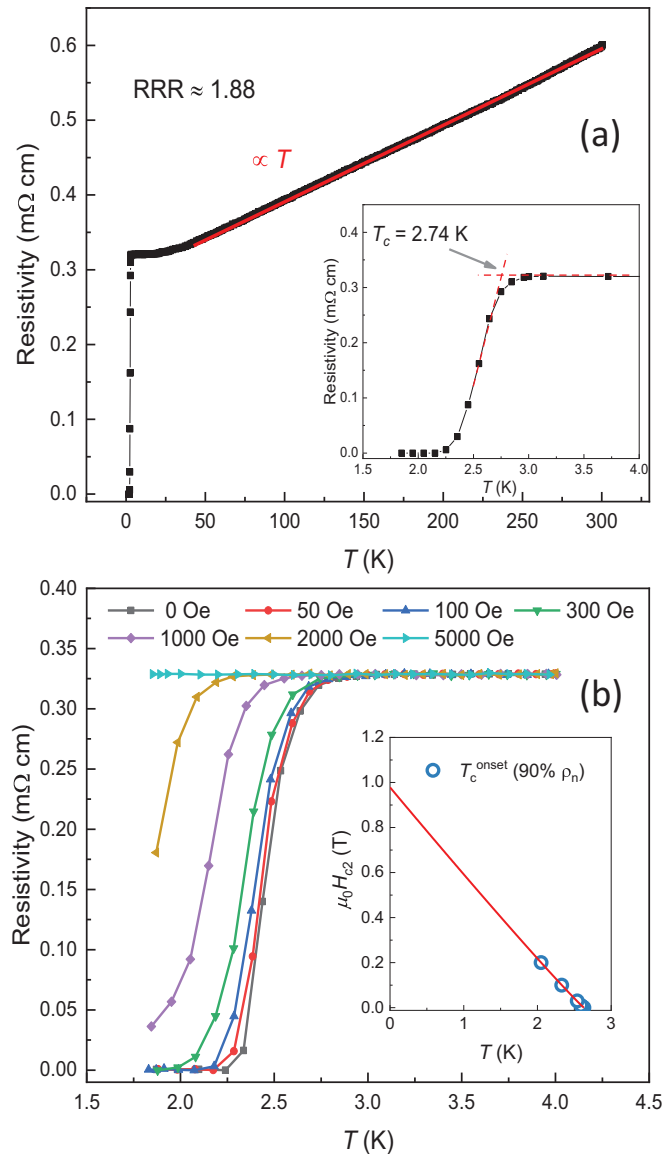

FIG. 3. (a) Temperature dependence of resistivity for 1T-PdSeTe. The inset shows an enlarged view of the resistivity near the superconducting transition temperature. (b) Temperature dependence of resistivity for 1T-PdSeTe at zero field and various magnetic fields parallel to the c axis. The inset shows the upper critical field H_{c2} as a function of temperature. The red line represents the best fitting using the function described in the text.

either an easy vortex motion with a weak flux pinning effect or a low charge carrier density in this system. The whole MHL indicates that 1T-PdSeTe is a type-II superconductor, in strong contrast to the type-I superconductivity found in the isostructural 1T-PdTe$_2$ compound [27]. In addition, the slopes for the perfect diamagnetism at 1.8 and 2 K are quite close to each other. The superconducting volume fraction estimated from the M-H curve is about 111%, which is quite close to the 103% estimated from the M-T results.

The temperature-dependent in-plane resistivity ρ_{ab} of 1T-PdSeTe is shown in Fig. 3(a). Resistivity decreases nearly linearly with temperature down to 50 K and keeps almost the same value when temperature continues to decrease to T_c.
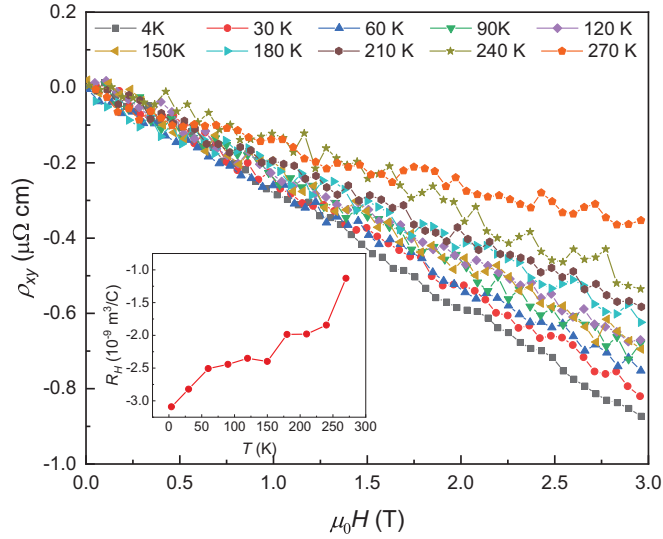
FIG. 4. Magnetic field dependence of the Hall resistivity ρ_{xy} for 1T-PdSeTe at various temperatures. The inset shows the temperature dependence of the Hall coefficient R_H.
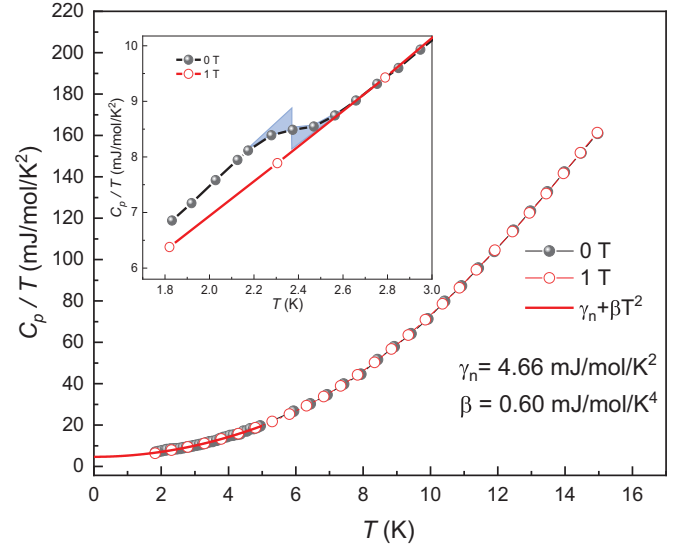

FIG. 5. Temperature dependence of specific heat under 0 T (solid circles) and 1 T (open circles). The red line represents the fitting using $C_p/T = \gamma_n + \beta T^2$. The inset shows an enlarged view of the temperature dependence of specific heat below 3 K. T_c is obtained utilizing the equal-area construction method for specific heat data.

The residual resistivity ratio (RRR), defined by R_{300K}/R_{4K}, is 1.88 for our 1T-PdSeTe samples. The RRR is smaller than that of pure PdTe$_2$ $\sim$ 30) [32], which is possibly due to the increase in electron scattering by lattice distortions or defects induced by Se doping. In the inset of Fig. 3(a), an enlarged view of resistivity near the transition temperature is presented, clearly showing the superconducting transition at about 2.74 K, which is a distinct 67% enhancement of T_c from that of PdTe$_2$ (1.64 K). Figure 3(b) shows the magnetic field dependence of resistivity for 1T-PdSeTe. T_c is gradually suppressed when the external field increases, a classical characteristic for superconductors. Taking a 10% resistivity drop as the criterion, the temperature dependence of the upper critical field H_{c2} is shown in the inset of Fig. 3(b). The upper critical field of 1T-PdSeTe shows a slightly positive curvature close to T_c, which is a characteristic of two-band clean-limit type-II superconductors and commonly exists in many layered superconductors, including MgB$_2$ [33], RNi$_2$B$_2$C [34,35] (R = rare-earth elements), and various superconducting TMDs. Consequently, the traditional Werthamer-Helfand-Hohenberg model, which normally has negative curvature close to T_c, does not fit the data very well. Experimentally, our H_{c2} can be fitted better in the entire T/T_c range using a semiempirical expression, $H_{c2}(T) = H^*_{c2}(1 - T/T_c)^{1+\alpha}$, previously applied to MgB$_2$, RNi$_2$B$_2$C, WTe$_2$, MoTe$_2$, and so on [12,33–36]. Note that the fitting parameters $B^*_{c2} = 0.97(2)$ T can be considered the upper limit for the upper critical field $B_{c2}(0)$. Thus, the Ginzburg-Landau coherence length $\xi_{GL}(0)$ can be estimated to be ~18 nm.

Figure 4 shows the temperature dependence of the Hall resistivity ρ_{xy} at 4, 30, 60, 90, 120, 150, 180, 210, 240, and 270 K at magnetic field up to 3 T. Here ρ_{xy} was measured with a longitudinal current. The magnetic field is perpendicular to the current and plate surface of 1T-PdSeTe samples. The voltage V_{xy} was measured in the direction across the sample width. As we can see, ρ_{xy} shows almost linearly dependent behavior with the magnetic field. The slope is completely

negative from 4 to 270 K, indicating that charge carriers are dominantly electrons at the Fermi surface. We estimated the Hall coefficient $R_H = \rho_{xy}/\mu_0 H$ by linearly fitting ρ_{xy} at various temperatures, as shown in the inset of Fig. 4. Further, R_H scales with the temperature almost monotonically, and such monotonic dependence behavior is consistent with many other TMD materials irrespective of the positive or negative sign of R_H [18]. The charge-carrier density estimated from $n = 1/(e \times R_H)$ is about 6.25×10^{21} cm^{-3} at 270 K and 1.95×10^{21} cm^{-3} at 4 K. Compared to the reported value of about 5.5×10^{21} cm^{-3} for PdTe$_2$ [27], the carrier density does not change too much as Se does not introduce extra carriers when doped at Te sites in PdTe$_2$. This further suggests that rather than the charge carriers, the admirable T_c enhancement might originate from other factors, which we will discuss further later.

In order to get more insights into the electronic and superconducting properties of our sample, we carried out the specific heat measurement. Figure 5 shows the raw data for the specific heat of 1T-PdSeTe at 0 and 1 T. Only a small specific heat anomaly appears in low-temperature region starting from 2.6 K, as shown in the inset of Fig. 5. This anomaly is coincident with the superconducting transition probed by resistivity and magnetization measurements. At 1 T, the superconductivity is completely suppressed, as suggested by the linear C$_p$/T vs T plot in the inset of Fig. 5. For 1T-PdSeTe, the normal state data can be fitted quite well using the Debye model $C_p/T = \gamma_n + \beta T^2$, which yields $\gamma_n = 4.66$ mJ mol^{-1} K^{-2}, $\beta = 0.60$ mJ mol^{-1} K^{-4}. The fitting curve is shown as the red line in Fig. 5. Debye temperature Θ_D can be calculated from the β value through the relationship $\Theta_D = [12\pi^4 N_A k_B Z/(5\beta)]^{1/3}$, where N_A is Avogadro's constant and Z is the number of atoms in one unit cell, which is 3 for 1T-PdSeTe. The obtained Debye temperature of 1T-PdSeTe

is about 213 K. It is worthwhile to note that the residual carrier contribution is estimated as $\gamma_0 = 3.71$ mJ mol^{-1} K^{-2} and the superconducting volume fraction therefore estimated from specific heat data is about $(\gamma_n - \gamma_0)/\gamma_n \approx 20\%$, which is quite consistent with the magnetic susceptibility measurement when $H//ab$ and further supports nonbulk superconductivity in this compound.

In addition, the derived Debye temperature for 1T-PdSeTe is slightly higher than that of PdTe$_2$ ($\Theta_D = 207$ K) single crystals [28]. The average electron-phonon coupling can be roughly estimated from the McMillan equation:

$$\lambda_{ep} = \frac{\mu^* \ln\left(\frac{1.45\, T_c}{\Theta_D}\right) - 1.04}{1.04 + \ln\left(\frac{1.45\, T_c}{\Theta_D}\right)(1 - 0.62\mu^*)}. \qquad (1)$$

Like for another TMD material, 2H-TaSe$_{2-x}$S$_x$ [13], we assume the empirical value of the Coulomb pseudopotential $\mu^* = 0.15$. Utilizing this Coulomb pseudopotential and the calculated Debye temperature, we can estimate λ_{ep} of 0.636 and 0.572 for 1T-PdSeTe and PdTe$_2$, respectively.

IV. DISCUSSION

The significantly enhanced T_c and nonbulk superconductivity in our 1T-PdSeTe sample are rather intriguing. Conventionally, the T_c enhancement is mainly caused by increasing charge carriers through chemical doping or physical pressure. However, our Hall measurement suggests that Se substitution does not introduce extra charge carriers. Although smaller Se substitution in the PdTe$_2$ lattice could cause the chemical pressure that plays a role similar to external pressure to tune the electronic structure, it is reported that the transition temperature of PdTe$_2$ can be enhanced only up to 1.91 K under an external pressure around 0.91 GPa. T_c, in fact, gradually decreases to 1.27 K when the external pressure reaches 2.5 GPa [32]. This further suggests that chemical pressure caused by Se substitution might not be sufficient to enhance T_c up to 2.74 K in the 1T-PdSeTe phase. On the other hand, the slightly larger λ_{ep} of 1T-PdSeTe (i.e., stronger electron-phonon coupling) than that of 1T-PdTe$_2$ might be supportive of T_c enhancement but cannot be the root cause for the enhanced superconductivity. Another possibility for this enhanced superconductivity could be lattice disorder and/or structural defects caused by Se doping. This phenomenon was been observed recently in many low-dimensional materials, including TMDs. For example, the superconducting transition temperature of TaS$_2$ can be enhanced from 2.89 to 3.61 K due to the disorder arising from the structural defects [37]. Bulk superconductivity with enhanced T_c was achieved in ZrTe$_3$ through growth-induced structural disorder [38]. To further elucidate such possibilities, we have carried out some control experiments as follows: three batches of samples with the same amount of reactants and the same heat treatments but three different cooling rates are presented. Specimen 1 (S1) samples are cooled in the furnace by turning off the power at 800 °C as shown before; specimen 2 (S2) undergoes slow cooling at a rate of 5 °C/h from 800 °C down to room temperature, which presumably should have the least grain boundaries and point defects, and specimen 3 (S3) samples are quenched into an ice water bath directly at 800 °C, whereby
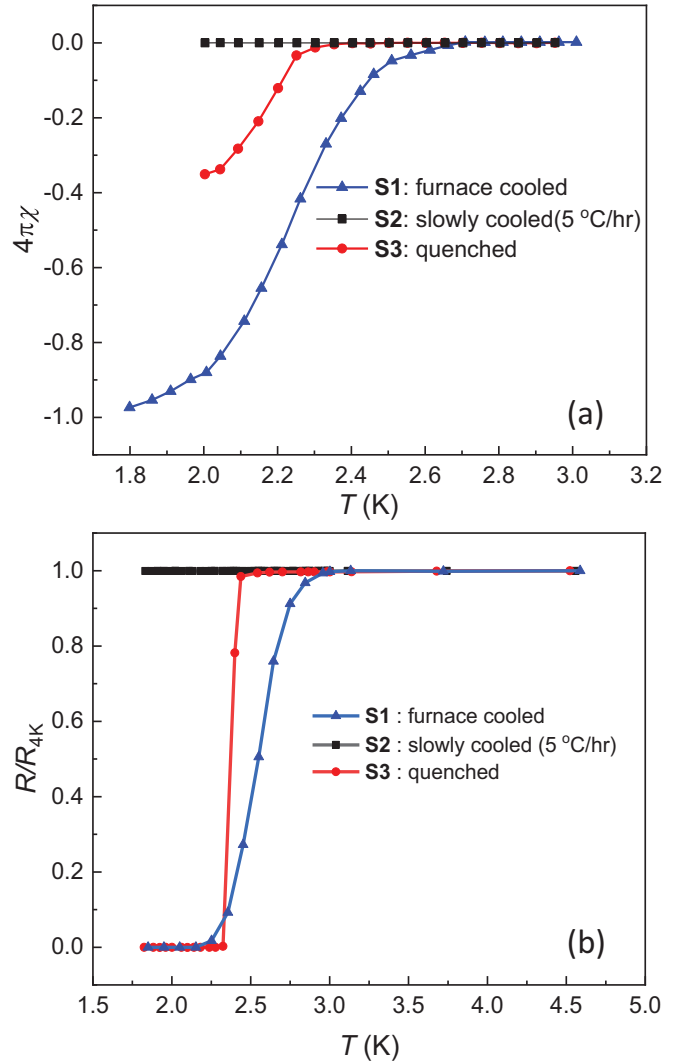

FIG. 6. (a) Temperature dependence of magnetization for 1T-PdSeTe near the superconducting phase transition with external magnetic field parallel to the c axis. The inset shows an enlarged view of the temperature-dependent magnetization of S2 and S3 in the ZFC mode. (b) Temperature dependence of normalized resistivity for 1T-PdSeTe synthesized under different cooling conditions.

the presence of structural disorder and defects should be the highest among all three specimens. Surprisingly, both S2 and S3 show worse superconductivity signals than S1. As shown in Fig. 6(a), under the same measurement condition where an external magnetic field is parallel to the c axis, no diamagnetic shielding (i.e., no superconductivity) is observed in the crystals from S2. And S3 is superconducting with a much smaller volume fraction ($\approx 35\%$) compared to that of S1 ($\sim 100\%$). This suggests that disorder/defects need to reach a certain threshold for the emergence of superconductivity with enhanced T_c, but certainly, too much disorder will be harmful for the superconductivity. On the other hand, from the resistivity measurement, it is quite interesting that S3, with a lower onset T_c, displays a much sharper superconducting transition than that of the S1 crystal. This is reminiscent of the behavior of Ru-rich Sr$_2$RuO$_4$ superconductors. T_c of Sr$_2$RuO$_4$ was raised from 1.5 to 3 K in Ru-rich samples with

a broader transition width, where excess Ru comes out of pure Sr_2RuO_4 and forms lamellar structures, typical of eutectic solidification [39]. Coincidentally, the 3 K Ru-rich phase is normally obtained through a faster growth rate than the 1.5 K phase for pure Sr_2RuO_4 samples. Further chemical analysis suggests that the three specimens have a slight difference in Se content in spite of the nearly identical Pd and Te composition. The ratio of Se content is S1:S2:S3 = 0.92(2):0.99(6):0.84(3). S1, with the highest T_c and volume fraction, has a slight Se deficiency, but apparently, the more Se deficient specimen S3 does not have better superconducting signals. Therefore, it is reasonable to speculate on several scenarios or maybe their combined effects that are responsible for the enhanced T_c in our furnace-cooled 1T-PdSeTe samples: (1) the possible existence of metallic Pd or PdTe stripes similar to Ru-Sr_2RuO_4 [39–41] and (2) some dedicated structural disorder caused by a rather small amount of Se deficiency [38,42,43]. The exact origin and mechanism could not be pinned down at this point unfortunately, which is left for future studies due to our current research constraints. It is also worthwhile to investigate whether the type-II Dirac band dispersion, as seen in the 1T-$PdTe_2$ phase, is preserved in this 1T-PdSeTe phase in the future through band structure calculation and advanced spectroscopy studies.

V. CONCLUSION

In conclusion, we have demonstrated that the superconducting transition temperature in the isostructural 1T-PdSeTe can be significantly enhanced to 2.74 K compared to the parent phase type-II Dirac semimetal $PdTe_2$ (1.64 K). The superconductivity has been investigated through resistivity, magnetization and specific heat measurements. Nonbulk superconductivity with a volume fraction of ∼20% was demonstrated by both magnetization and specific heat data. The possibilities of substantial T_c enhancement arising from the possible existence of metallic Pd or PdTe stripes similar to Ru-Sr_2RuO_4 and/or some dedicated structural disorder caused by a rather small amount of Se deficiency were examined and discussed.

[1] K. S. Novoselov, A. Mishchenko, A. Carvalho, and A. H. Castro Neto, Science **353**, aac9439 (2016)

[2] Y. Liu, N. O. Weiss, X. Duan, H.-C. Cheng, Y. Huang, and X. Duan, Nat. Rev. Mater. **1**, 16042 (2016).

[3] M. Chhowalla, H. S. Shin, G. Eda, L. J. Li, K. P. Loh, and H. Zhang, Nat. Chem. **5**, 263 (2013).

[4] J. Li *et al.*, Nature (London) **579**, 368 (2020).

[5] B. Radisavljevic and A. Kis, Nat. Mater. **12**, 815 (2013).

[6] D. H. Keum, S. Cho, J. H. Kim, D.-H. Choe, H.-J. Sung, M. Kan, H. Kang, J.-Y. Hwang, S. W. Kim, H. Yang, K. J. Chang, and Y. H. Lee, Nat. Phys. **11**, 482 (2015).

[7] Y. Luo, H. Li, Y. M. Dai, H. Miao, Y. G. Shi, H. Ding, A. J. Taylor, D. A. Yarotski, R. P. Prasankumar, and J. D. Thompson, Appl. Phys. Lett. **107**, 182411 (2015).

[8] C. Gong and X. Zhang, Science **363**, eaav4450 (2019).

[9] M. Bonilla, S. Kolekar, Y. Ma, H. C. Diaz, V. Kalappattil, R. Das, T. Eggers, H. R. Gutierrez, M.-H. Phan, and M. Batzill, Nat. Nanotechnol. **13**, 289 (2018).

[10] R. A. Klemm, Phys. C (Amsterdam, Neth.) **514**, 86 (2015).

[11] H. Wu, S. Li, M. Susner, S. Kwon, M. Kim, T. Haugan, and B. Lv, 2D Mater. **6**, 045048 (2019).

[12] Y. Qi *et al.*, Nat. Commun. **7**, 11038 (2016).

[13] L. Li, X. Deng, Z. Wang, Y. Liu, M. Abeykoon, E. Dooryhee, A. Tomic, Y. Huang, J. B. Warren, E. S. Bozin, S. J. L. Billinge, Y. Sun, Y. Zhu, G. Kotliar, and C. Petrovic, npj Quantum Mater. **2**, 11 (2017).

[14] Y. Liu, D. F. Shao, L. J. Li, W. J. Lu, X. D. Zhu, P. Tong, R. C. Xiao, L. S. Ling, C. Y. Xi, L. Pi, H. F. Tian, H. X. Yang, J. Q. Li, W. H. Song, X. B. Zhu, and Y. P. Sun, Phys. Rev. B **94**, 045131 (2016).

[15] R. Zhang, I. L. Tsai, J. Chapman, E. Khestanova, J. Waters, and I. V. Grigorieva, Nano Lett. **16**, 629 (2016).

[16] Y. Yu, F. Yang, X. F. Lu, Y. J. Yan, Y. H. Cho, L. Ma, X. Niu, S. Kim, Y. W. Son, D. Feng, S. Li, S. W. Cheong, X. H. Chen, and Y. Zhang, Nat. Nanotechnol. **10**, 270 (2015).

[17] D. Costanzo, S. Jo, H. Berger, and A. F. Morpurgo, Nat. Nanotechnol. **11**, 339 (2016).

[18] X. Xi, H. Berger, L. Forró, J. Shan, and K. F. Mak, Phys. Rev. Lett. **117**, 106801 (2016).

[19] X. Che, Y. Deng, Y. Fang, J. Pan, Y. Yu, and F. Huang, Adv. Electron. Mater. **5**, 1900462 (2019).

[20] S. C. De La Barrera, M. R. Sinko, D. P. Gopalan, N. Sivadas, K. L. Seyler, K. Watanabe, T. Taniguchi, A. W. Tsen, X. Xu, D. Xiao, and B. M. Hunt, Nat. Commun. **9**, 1427 (2018).

[21] T. Dvir, F. Massee, L. Attias, M. Khodas, M. Aprili, C. H. L. Quay, and H. Steinberg, Nat. Commun. **9**, 598 (2018).

[22] S. Ulstrup, R. J. Koch, S. Singh, K. M. McCreary, B. T. Jonker, J. T. Robinson, C. Jozwiak, E. Rotenberg, A. Bostwick, J. Katoch, and J. A. Miwa, Sci. Adv. **6**, eaay6104 (2020).

[23] E. C. Regan, D. Wang, C. Jin, M. I. Bakti Utama, B. Gao, X. Wei, S. Zhao, W. Zhao, Z. Zhang, K. Yumigeta, M. Blei, J. D. Carlström, K. Watanabe, T. Taniguchi, S. Tongay, M. Crommie, A. Zettl, and F. Wang, Nature (London) **579**, 359 (2020).

[24] O. J. Clark, M. J. Neat, K. Okawa, L. Bawden, I. Marković, F. Mazzola, J. Feng, V. Sunko, J. M. Riley, W. Meevasana, J. Fujii, I. Vobornik, T. K. Kim, M. Hoesch, T. Sasagawa, P. Wahl, M. S. Bahramy, and P. D. C. King, Phys. Rev. Lett. **120**, 156401 (2018).

[25] H. J. Noh, J. Jeong, E. J. Cho, K. Kim, B. I. Min, and B. G. Park, Phys. Rev. Lett. **119**, 016401 (2017).

[26] J. Guggenheim, F. Hulliger, and J. H. Muller, Helv. Phys. Acta **34**, 408 (1961).

[27] H. Leng, C. Paulsen, Y. K. Huang, and A. de Visser, Phys. Rev. B **96**, 220506(R) (2017).

[28] Amit and Y. Singh, Phys. Rev. B **97**, 054515 (2018).

[29] Y. Liu, Y. Xu, J. Sun, C. Liu, Y. Liu, C. Wang, Z. Zhang, K. Gu, Y. Tang, C. Ding, H. Liu, H. Yao, X. Lin, L. Wang, Q.-K. Xue, and J. Wang, Nano Lett. **20**, 5728 (2020).

[30] F. Hulliger, J. Phys. Chem. Solids **26**, 639 (1965)

[31] B. H. Toby and R. B. Von Dreele, J. Appl. Crystallogr. **46**, 544 (2013).

[32] H. Leng, A. Ohmura, L. N. Anh, F. Ishikawa, T. Naka, Y. K. Huang, and A. De Visser, J. Phys.: Condens. Matter **32**, 025603 (2020).

[33] K. H. Muller, G. Fuchs, A. Handstein, K. Nenkov, V. N. Narozhnyi, and D. Eckert, J. Alloys Compd. **322**, 10 (2001).

[34] S. V. Shulga, S. L. Drechsler, G. Fuchs, and K.-H. Müller, K. Winzer, M. Heineche, and K. Krug, Phys. Rev. Lett. **80**, 1730 (1998).

[35] J. Freudenberger, S. L. Drechsler, G. Fuchs, A. Kreyssig, K. Nenkov, S. V. Shulga, K. H. Muller, and L. Schultz, Phys. C (Amsterdam, Neth.) **306**, 1 (1998).

[36] X. C. Pan, X. Chen, H. Liu, Y. Feng, Z. Wei, Y. Zhou, Z. Chi, L. Pi, F. Yen, F. Song, X. Wan, Z. Yang, B. Wang, G. Wang, and Y. Zhang, Nat. Commun. **6**, 7805 (2015).

[37] J. Peng, Z. Yu, J. Wu, Y. Zhou, Y. Guo, Z. Li, J. Zhao, C. Wu, and Y. Xie, ACS Nano **12**, 9461 (2018).

[38] X. Zhu, B. Lv, F. Wei, Y. Xue, B. Lorenz, L. Deng, Y. Sun, and C. W. Chu, Phys. Rev. B **87**, 024508 (2013).

[39] Y. Maeno, T. Ando, Y. Mori, E. Ohmichi, S. Ikeda, S. NishiZaki, and S. Nakatsuji, Phys. Rev. Lett. **81**, 3765 (1998).

[40] M. Sigrist and H. Monien, J. Phys. Soc. Jpn. **70**, 2409 (2001).

[41] H. Kaneyasu, N. Hayashi, B. Gut, K. Makoshi, and M. Sigrist, J. Phys. Soc. Jpn. **79**, 104705 (2010).

[42] M. N. Gastiasoro and B. M. Andersen, Phys. Rev. B **98**, 184510 (2018).

[43] M. Hoesch, L. Gannon, K. Shimada, B. J. Parrett, M. D. Watson, T. K. Kim, X. Zhu, and C. Petrovic, Phys. Rev. Lett. **122**, 017601 (2019).